

Distribution-Aware Calibration for Object Detection with Noisy Bounding Boxes

Donghao Zhou^{1,2,3*}, Jialin Li⁴, Jinpeng Li³, Jiancheng Huang^{1,2}, Qiang Nie⁴, Yong Liu^{4†},
Bin-Bin Gao⁴, Qiong Wang¹, Pheng-Ann Heng^{1,3,5}, Guangyong Chen^{5†}

¹Shenzhen Institute of Advanced Technology, Chinese Academy of Sciences

²University of Chinese Academy of Sciences ³The Chinese University of Hong Kong

⁴Tencent YouTu Lab ⁵Zhejiang Lab

Abstract

Large-scale well-annotated datasets are of great importance for training an effective object detector. However, obtaining accurate bounding box annotations is laborious and demanding. Unfortunately, the resultant noisy bounding boxes could cause corrupt supervision signals and thus diminish detection performance. Motivated by the observation that the real ground-truth is usually situated in the aggregation region of the proposals assigned to a noisy ground-truth, we propose DIStribution-aware CalibratiOn (DISCO) to model the spatial distribution of proposals for calibrating supervision signals. In DISCO, spatial distribution modeling is performed to statistically extract the potential locations of objects. Based on the modeled distribution, three distribution-aware techniques, *i.e.*, distribution-aware proposal augmentation (DA-Aug), distribution-aware box refinement (DA-Ref), and distribution-aware confidence estimation (DA-Est), are developed to improve classification, localization, and interpretability, respectively. Extensive experiments on large-scale noisy image datasets (*i.e.*, Pascal VOC and MS-COCO) demonstrate that DISCO can achieve state-of-the-art detection performance, especially at high noise levels.

1 Introduction

Object detection has made substantial progress in recent years (Ren et al. 2015; Lin et al. 2017b; Carion et al. 2020; Sun et al. 2021; Zou et al. 2023), which is largely attributed to the utilization of large-scale well-annotated datasets (Everingham et al. 2010; Lin et al. 2014). However, obtaining accurate bounding box annotations is labor-intensive and demanding, especially for some real-world scenarios such as medical diagnosis (Luo et al. 2021; Chai et al. 2023) and autonomous driving (Michaelis et al. 2019; Mao et al. 2022). As shown in Figure 1(a), inherent ambiguities of bounding boxes are often caused by object occlusion or unclear boundaries (He et al. 2019). Moreover, insufficient domain expertise and the strenuous workload can also lead to low-quality labeling of bounding boxes (Liu et al. 2022). In practical deployments and applications, vanilla object detectors will inevitably suffer from such noisy bounding box annotations. Therefore, it is of scientific interest to explore how to tackle noisy bounding boxes in object detection.

*Work was done during an internship at Tencent YouTu Lab.

†Corresponding authors.

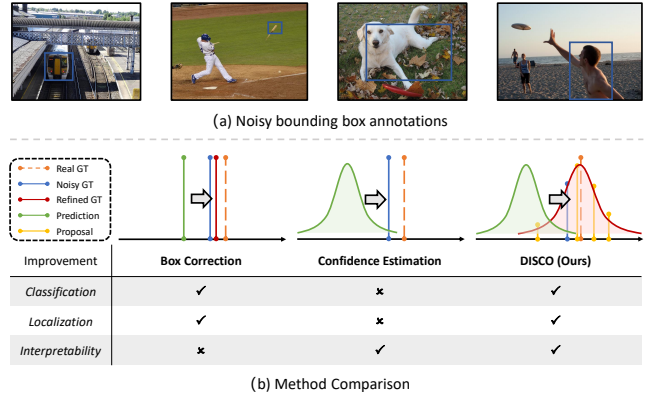


Figure 1: (a) Examples of noisy bounding box annotations. For simplicity, the noisy annotation for one object is presented per image. (b) Comparison of existing solutions and the proposed method. We present their learning behaviors for one single border of bounding boxes as an illustration.

Due to the degenerated supervision introduced by noisy annotations, object detection with noisy bounding boxes remains a challenging problem. Obviously, such corrupt supervision signals could weaken the localization precision of object detectors. Besides, although the classification accuracy is less affected (Liu et al. 2022), noisy bounding boxes do introduce biased category features during training, which reduces the generalization capability of classification. Notably, there is also a significant concern about the lack of interpretability for box predictions, especially considering the influence of noisy bounding box annotations.

Encountering the above challenges, existing solutions still exhibit drawbacks in this special setting (see Figure 1(b)). Several previous works are dedicated to correcting noisy bounding boxes (Liu et al. 2022; Li et al. 2020a; Xu et al. 2021), aiming to mitigate the effect of noisy box annotations. However, their performance gains in classification and localization are constrained by heuristic box correction approaches, and the detector cannot identify which bounding boxes are inaccurately predicted. An alternative series of methods focus on equipping the model with the capability to estimate the confidence of predicted bounding boxes (He et al. 2019; Li et al. 2020b; Choi et al. 2019), through which

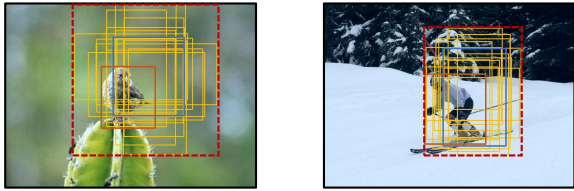


Figure 2: Examples of proposal aggregation in object detection with noisy bounding boxes. Real ground-truths, noisy ground-truths, and the assigned proposals are marked in orange, blue, and yellow, respectively. Note that the aggregation regions of the assigned proposals are indicated by red dashed rectangles.

the detector can be more robust against noisy box annotations. Despite these efforts, it is unfortunate that the detector is still plagued by flawed supervision during training.

Essentially, the corrupt supervision signals should be blamed for the above issues. In this work, we expect to answer the following question: *How to properly calibrate the corrupt supervision signals?* As shown in Figure 2, we observed that the real ground-truth is usually situated in the aggregation region of the proposals assigned to a noisy ground-truth. Furthermore, the proposals are more densely aggregated around a reliable one, showing that the spatial distribution of proposals can act as a statistical prior for the potential locations of objects. Thus, we propose *DISTRIBUTION-AWARE CALIBRATION (DISCO)*, which aims to model the spatial *distribution* of proposals for *calibrating* supervision signals (see Figure 1(b)). For each group of the assigned proposals, we perform *spatial distribution modeling* with a four-dimensional Gaussian distribution, statistically extracting potential locations of objects. Based on the modeled distribution, we develop three distribution-aware techniques to improve *classification*, *localization*, and *interpretability*, respectively: 1) *Distribution-aware proposal augmentation (DA-Aug)*: Additional proposals are generated from the distribution to enrich category features in the representative locations, and then the proposal with the highest classification score is collected to boost classification performance; 2) *Distribution-aware box refinement (DA-Ref)*: With a non-linear weighting strategy, noisy ground-truth is fused with the distribution into a refined ground-truth to achieve superior bounding box regression; 3) *Distribution-aware confidence estimation (DA-Est)*: An extra estimator is integrated into the detection head, with the distribution variance elegantly acting as its supervision, to estimate the confidence of predicted bounding boxes for better non-maximum suppression (NMS). Without introducing complicated learnable modules, DISCO can attain state-of-the-art performance on large-scale noisy image datasets (*i.e.*, Pascal VOC and MSCOCO), especially at high noise levels. Our main contributions are summarized as follows:

- Motivated by the observation about proposal aggregation, we propose an approach called DISCO to calibrate supervision signals with spatial distribution modeling.
- To improve classification, localization, and interpretability, we introduce three techniques (*i.e.*, DA-Aug, DA-

Ref, and DA-Est) to collaborate with the modeled distribution in a distribution-aware manner.

- Comprehensive experiments show that our DISCO can attain state-of-the-art performance in object detection with noisy bounding boxes and meanwhile achieve satisfactory interpretability for its predictions.

2 Related Works

2.1 Object Detection

The goal of object detection is to recognize what objects are present and where they are situated. Faster-RCNN (Ren et al. 2015) is a classic detection framework with a two-stage strategy, and is widely adopted and improved in subsequent works (Cai and Vasconcelos 2018; Pang et al. 2019; Sun et al. 2021). On the other hand, RetinaNet (Lin et al. 2017b) delves into efficient loss design to strengthen the performance of one-stage detectors. Recently, transformer-based detectors (Carion et al. 2020; Zhu et al. 2020; Zhang et al. 2022) also attract the attention of the community, which conducts object detection in an end-to-end fashion. Training with accurate bounding box annotations, object detectors can achieve satisfactory and even remarkable performance. However, object detection with noisy bounding boxes remains an under-explored subproblem.

2.2 Object Detection with Noisy Annotations

Specifically, noisy annotations of an object detection dataset could compose of noisy category labels and noisy bounding boxes. Previous works (Chadwick and Newman 2019; Li et al. 2020a; Xu et al. 2021) have made attempted to jointly tackle these two types of noisy annotations. Unlike this setting, we focus on training an object detector with noisy bounding boxes, since box noise is more common and challenging in realistic scenarios (Liu et al. 2022). The state-of-the-art for this tough task is called OA-MIL (Liu et al. 2022), which adopts a multi-instance learning (MIL) framework at the object level to correct bounding boxes. Besides, some approaches aiming to boost the robustness of detectors, such as KL Loss (He et al. 2019), can also contribute to performance improvement in this task.

2.3 Weakly Supervised Object Detection

Weakly supervised object detection (WSOD) is also a relevant task, where only image-level labels can be accessed to train an object detector. The mainstream solution is to treat WSOD as a MIL problem (Bilen and Vedaldi 2016; Wan et al. 2018; Chen et al. 2020; Tang et al. 2017), where each training image is constructed as a bag of instances. To handle the non-convex optimization of MIL, spatial regularization (Diba et al. 2017; Wan et al. 2018), optimization strategy (Tang et al. 2017; Wan et al. 2019), and context information (Kantorov et al. 2016; Wei et al. 2018) are introduced to attain better convergence. Moreover, it is worth noting that SD-LocNet (Zhang, Yang, and Feng 2019) contributes a self-directed optimization strategy to handle object instances with noisy initial locations. Unfortunately, WSOD always results in relatively inaccurate box predictions due to

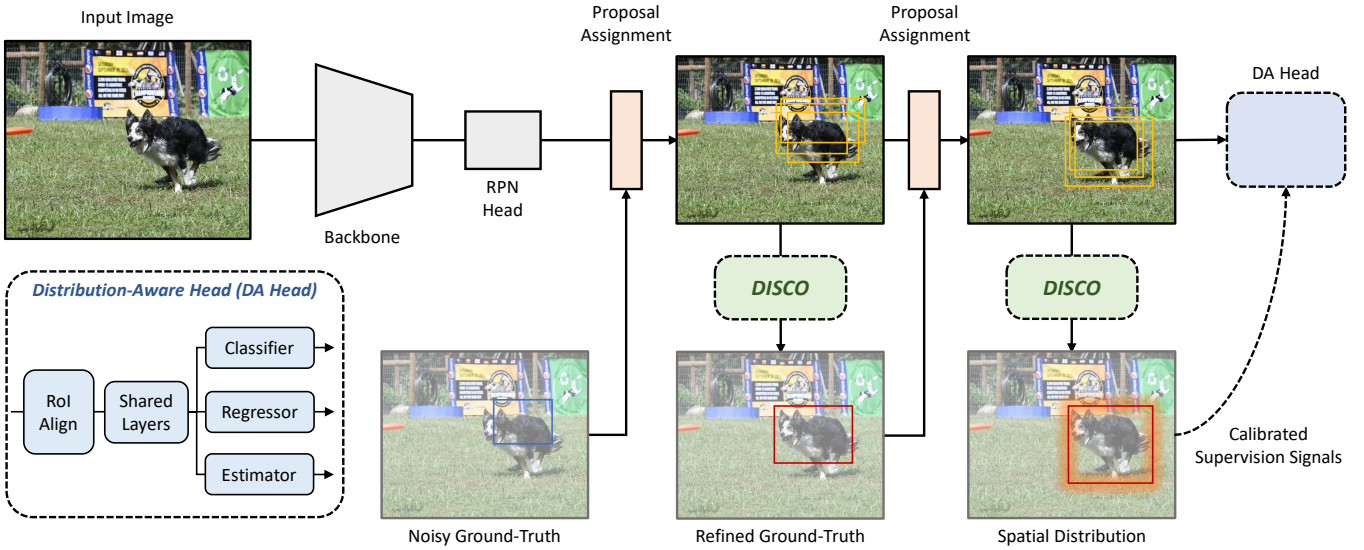


Figure 3: Training pipeline with the proposed DISCO. Note that DISCO is performed twice in a training iteration, the first time for proposal reassignment and the second time for producing calibrated supervision signals.

the lack of fine-grained supervision. Effective methods for object detection with noisy bounding boxes have the potential to further refine these predictions.

3 Methodology

In this work, we propose DISCO to calibrate the corrupt supervision signals caused by noisy bounding boxes in object detection. In essence, DISCO is an online calibration approach during the training phase. Notably, we integrate an estimator into the vanilla detection head to construct the distribution-aware head (DA head). In a training iteration, DISCO is performed twice using the DA head with the assigned proposals as input (see Figure 3). The first time aims to yield a refined ground-truth for proposal reassignment, by which better-matching proposals can be obtained. The second time aims to produce spatial distributions of proposals acting as superior supervision. In the following, we start by describing spatial distribution modeling in Section 3.1. Then, we will introduce three distribution-aware techniques (*i.e.*, DA-Aug, DA-Ref, and DA-Est) in Section 3.2, 3.3 and 3.4, respectively, in which we will also detail the differences between these two times of DISCO.

3.1 Spatial Distribution Modeling

In DISCO, spatial distribution modeling is conducted for each group of the proposals assigned to a noisy/refined ground-truth (see Figure 4). Let $\mathbf{P}^i = [P_1^i, P_2^i, \dots, P_{N^i}^i] \in \mathbb{R}^{N^i \times 4}$ denotes the i -th group of the proposals, where N^i is the number of the proposals in \mathbf{P}^i . Moreover, \mathbf{P}^i is associated with a category indicator $l^i \in \{1, 2, \dots, L\}$ where L is the number of categories. Note that the noisy ground-truth is included in \mathbf{P}^i as commonly done, and each proposal $P_j^i \in \mathbb{R}^4$ represents four coordinates of bounding boxes.

First, the features of the proposals in \mathbf{P}^i are extracted as

$$\mathbf{F}^i = \mathcal{F}(\mathbf{P}^{i*}, \mathbf{X}) = [F_1^i, F_2^i, \dots, F_{N^i}^i] \in \mathbb{R}^{N^i \times D}, \quad (1)$$

where $\mathcal{F}(\cdot, \cdot)$ is the joint operation of RoIAlign (He et al. 2017) and two shared fully connected (FC) layers and \mathbf{X} is the feature maps produced by the backbone. As a result, each proposal P_j^i corresponds to a D -dimensional feature vector F_j^i . Then, we adopt the regressor $\mathcal{R}(\cdot)$ of the DA head to predict proposal offsets for further localization and update the features, which is formulated as

$$\mathbf{P}^{i*} = \text{Trans}(\mathbf{P}^i, \mathcal{R}(\mathbf{F}^i)) \in \mathbb{R}^{N^i \times 4}, \quad (2)$$

$$\mathbf{F}^{i*} = \mathcal{F}(\mathbf{P}^{i*}, \mathbf{X}) \in \mathbb{R}^{N^i \times D}, \quad (3)$$

where $\text{Trans}(\cdot, \cdot)$ is a function that translates predicted offsets to proposals. Following (Liu et al. 2022), we utilize classification scores to measure the possibilities of object locations. Therefore, the classifier $\mathcal{C}(\cdot)$ is used to score the proposals \mathbf{F}^{i*} , which is defined as

$$\mathbf{S}^i = \mathcal{C}(\mathbf{F}^{i*}) \in \mathbb{R}^{N^i \times (L+1)}, \quad (4)$$

$$S^i = \text{LookUp}(\mathbf{S}^i, l^i) = [s_1^i, s_2^i, \dots, s_{N^i}^i] \in \mathbb{R}^{N^i}, \quad (5)$$

where $\text{LookUp}(\cdot, \cdot)$ is a look-up operation that extracts the l^i -th column from \mathbf{S}^i , and the resultant S^i denotes the classification scores of the corresponding category. Subsequently, we utilize S^i to produce the normalized weights W^i for the proposals \mathbf{F}^{i*} , expressed as

$$W^i = \text{Softmax}(S^i, T) = [w_1^i, w_2^i, \dots, w_{N^i}^i] \in \mathbb{R}^{N^i}, \quad (6)$$

where $\text{Softmax}(\cdot, \cdot)$ is the Softmax function and T is its temperature coefficient (Hinton, Vinyals, and Dean 2015). Finally, we model the spatial distribution of \mathbf{P}^{i*} as a four-dimensional Gaussian distribution by directly calculating its

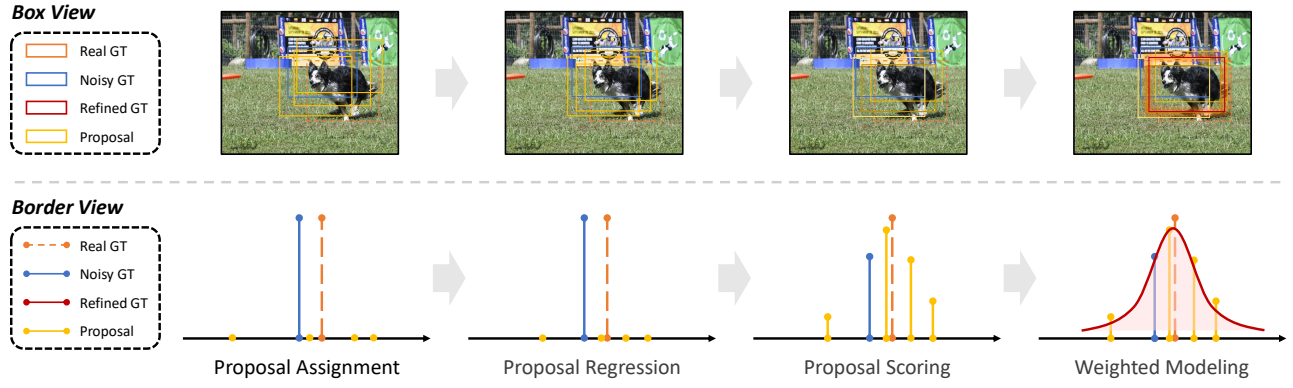


Figure 4: Illustration of spatial distribution modeling. For clarity, we present the process of spatial distribution modeling in the view of the whole bounding box or one single border. Note that the length of the vertical line indicates its weight.

parameters (*i.e.*, mean μ^i and standard deviation σ^i) in a weighting manner, which can be formulated as

$$\mu^i = \sum_{j=1}^{N^i} w_j^i * P_j^{i*} \in \mathbb{R}^4, \quad (7)$$

$$\sigma^i = \sqrt{\sum_{j=1}^{N^i} w_j^i * (P_j^i - \mu^i)^2} \in \mathbb{R}^4, \quad (8)$$

where we assume that each dimension of this Gaussian distribution is uncorrelated so that its standard deviation can be formulated as a four-dimensional vector.

3.2 Distribution-Aware Proposal Augmentation

Instead of using heuristic approaches such as selective search (Uijlings et al. 2013) and edge box (Zitnick and Dollár 2014), we propose to augment proposals with the modeled distribution, aiming to statistically cover more potential locations of objects. Firstly, we create a Gaussian noise matrix $\mathbf{G} \in \mathbb{R}^{N' \times 4}$ whose each element is sampled from $\mathcal{N}(0, 1)$ to ensure randomness. Here N' is a hyperparameter that indicates the number of augmented proposals. Then, augmented proposals $\mathbf{P}^{i'}$ can be generated by

$$\mathbf{P}^{i'} = \mu^i + \mathbf{G} \odot \sigma^i = [P_1^{i'}, P_2^{i'}, \dots, P_{N'}^{i'}] \in \mathbb{R}^{N' \times 4}, \quad (9)$$

where \odot denotes element-wise multiplication and the operations here are all conducted in a broadcasting fashion. Following Equation 4 and 5, its classification scores $S^{i'}$ can be obtained. Subsequently, we incorporate the augmented proposals $\mathbf{P}^{i'}$ into \mathbf{P}^i , expressed as

$$\mathbf{P}^{i*} \leftarrow \mathbf{P}^{i*} \oplus \mathbf{P}^{i'} \in \mathbb{R}^{(N^i + N') \times 4}, \quad (10)$$

$$S^i \leftarrow S^i \oplus S^{i'} \in \mathbb{R}^{N^i + N'}, \quad (11)$$

where \oplus indicates proposal-wise concatenation. To boost classification performance, the proposals with the highest classification score, which could contain representative category features, are collected to form a loss term for classification, formulated as

$$s_*^i = \max_j s_j^i, \quad j = 1, 2, \dots, (N^i + N'), \quad (12)$$

$$\mathcal{L}_{\text{Aug}} = -\frac{1}{M} \sum_{i=1}^M \log(s_*^i), \quad (13)$$

where M is the number of proposal groups in a batch. Note that \mathcal{L}_{Aug} does not be computed in the first-time DISCO. Finally, after proposal augmentation, we follow Equation 7 and 8 to model the spatial distribution of \mathbf{P}^{i*} once again for a better representation of these proposals.

3.3 Distribution-Aware Box Refinement

As we mentioned before, the model spatial distribution can be considered as a statistical prior for the potential locations of objects. Therefore, it can act as guidance for noisy bounding box refinement. First, we treat μ^i as a proposal, extract its feature with $\mathcal{F}(\cdot, \cdot)$, and adopt the classifier $\mathcal{C}(\cdot)$ to obtain its classification score s_μ^i . Then, the noisy bounding box B^i is refined as $B^{i'}$ by a fusion strategy as

$$B^{i'} = \phi(s_\mu^i) \cdot \mu^i + (1 - \phi(s_\mu^i)) \cdot B^i, \quad (14)$$

where $\phi(\cdot)$ is a non-linear weighting function following (Liu et al. 2022). To stabilize the early stage of training, the fusion strategy is conditional on the classification score s_μ^i , and thus the $\phi(\cdot)$ is defined as

$$\phi(s_\mu^i) = \min((s_\mu^i)^\alpha, \beta), \quad (15)$$

where α and β are two hyperparameters. Finally, the refined $B^{i'}$ is used as supervision for the original proposals \mathbf{P}^i to compute regression loss as

$$\mathcal{L}_{\text{reg}} = \frac{1}{M} \sum_{i=1}^M \frac{1}{N^i} \sum_{j=1}^{N^i} \text{Dist}(P_j^i, B^{i'}), \quad (16)$$

where $\text{Dist}(\cdot, \cdot)$ is a predefined distance function for two bounding boxes (Ren et al. 2015). It is worth noting that the first-time DISCO is ended with Equation 14 to obtain the refined ground-truth $B^{i'}$ for proposal reassignment.

3.4 Distribution-Aware Confidence Estimation

To estimate the confidence of predicted bounding boxes, we integrate an estimator $\mathcal{E}(\cdot)$ into the DA head. The confidence

Method	VOC				COCO											
	Box Noise Level				20% Box Noise Level						40% Box Noise Level					
	10%	20%	30%	40%	AP	AP ₅₀	AP ₇₅	AP _S	AP _M	AP _L	AP	AP ₅₀	AP ₇₅	AP _S	AP _M	AP _L
Clean-FasterRCNN	77.2	77.2	77.2	77.2	37.9	58.1	40.9	21.6	41.6	48.7	37.9	58.1	40.9	21.6	41.6	48.7
Clean-RetinaNet	73.5	73.5	73.5	73.5	36.7	56.1	39.0	21.6	40.4	47.4	36.7	56.1	39.0	21.6	40.4	47.4
FasterRCNN	76.3	71.2	60.1	42.5	30.4	54.3	31.4	17.4	33.9	38.7	10.3	28.9	3.3	5.7	11.8	15.1
RetinaNet	71.5	67.5	57.9	45.0	30.0	53.1	30.8	17.9	33.7	38.2	13.3	33.6	5.7	8.4	15.9	18.0
Co-teaching	75.4	70.6	60.9	43.7	30.5	54.9	30.5	17.3	34.0	39.1	11.5	31.4	4.2	6.4	13.1	16.4
SD-LocNet	75.7	71.5	60.8	43.9	30.0	54.5	30.3	17.5	33.6	38.7	11.3	30.3	4.3	6.0	12.7	16.6
FreeAnchor	73.0	67.5	56.2	41.6	28.6	53.1	28.5	16.6	32.2	37.0	10.4	28.9	3.3	5.8	12.1	14.9
KL Loss	75.8	72.7	64.6	48.6	31.0	54.3	32.4	18.0	34.9	39.5	12.1	36.7	3.7	6.2	13.0	17.4
OA-MIL	77.4	74.3	70.6	63.8	32.1	55.3	33.2	18.1	35.8	41.6	18.6	42.6	12.9	9.2	19.0	26.5
DISCO (Ours)	77.5	75.3	72.1	68.7	32.3	54.7	34.5	18.7	35.8	41.2	21.2	45.7	16.9	11.4	24.7	27.8

Table 1: Benchmark results of our DISCO and the comparing methods on VOC and COCO, where the best performance is marked in bold. Note that Clean-FasterRCNN/RetinaNet denotes the detectors trained with clean annotations for reference.

\mathbf{V}^i for the proposals \mathbf{P}^i can be produced as

$$\mathbf{V}^i = \mathcal{E}(\mathbf{F}^i) = [V_1^i, V_2^i, \dots, V_{N^i}^i] \in \mathbb{R}^{N^i \times 4}. \quad (17)$$

As shown in Figure 2, it can be observed that the proposals are more densely aggregated around a reliable ground-truth. Notably, the aggregation level can be measured by the variance (or standard deviation) of the modeled spatial distribution. Therefore, the distribution variance can be elegantly adopted as the supervision of the estimator $\mathcal{E}(\cdot)$. The loss for training $\mathcal{E}(\cdot)$ is formulated as

$$\mathcal{L}_{\text{Est}} = \frac{1}{M} \sum_{i=1}^M \frac{1}{N^i} \sum_{j=1}^{N^i} \|V_j^i - (\sigma^i)^2\|_1. \quad (18)$$

Different from (He et al. 2019), we train the estimator with direct supervision of variance rather than implicit supervision of bounding boxes. Then, the estimated confidence (*i.e.*, predicted variance) is used in Softer-NMS (He et al. 2019) for a better inference-time process. Finally, the overall loss function is formed as

$$\mathcal{L}_{\text{All}} = \mathcal{L}_{\text{Cls}} + \mathcal{L}_{\text{Reg}} + \gamma \mathcal{L}_{\text{Est}} + \lambda \mathcal{L}_{\text{Aug}}, \quad (19)$$

where γ and λ is two hyperparameters to down-weight \mathcal{L}_{Est} and \mathcal{L}_{Aug} respectively, and \mathcal{L}_{Cls} is a cross-entropy classification loss for the original proposals \mathbf{P}^i (Ren et al. 2015).

4 Experiments

4.1 Experimental Setup

Datasets. Two large-scale image datasets are adopted in the experiments, including Pascal VOC 2007 (Everingham et al. 2010) and MS-COCO 2017 (Lin et al. 2014). Pascal VOC 2007 (VOC) is a standard dataset for object detection, consisting of 9,963 images with 24,640 box annotations. MS-COCO 2017 (COCO) is also a popular object detection benchmark, containing 328,000 images of

generic objects. Following (Liu et al. 2022), noisy bounding box annotations are simulated by perturbing clean ones at various noise levels. Specifically, the noise levels are set to $\{10\%, 20\%, 30\%, 40\%\}$ for VOC and $\{20\%, 40\%\}$ for COCO. More details are provided in the appendix.

Implementation Details. Following (Liu et al. 2022), we implement our method on FasterRCNN (Ren et al. 2015) with ResNet-50-FPN backbone (He et al. 2016; Lin et al. 2017a). As a common practice, the model is trained with the “1×” schedule (Girshick et al. 2018). Hyperparameter selections of our method are detailed in the appendix. Notably, all other training configurations are aligned with (Liu et al. 2022) to ensure fairness.

Evaluation Metrics. As commonly done, mean average precision (mAP@.5) and mAP@[.5, 95] are used for VOC and COCO respectively. Specifically, we report AP₅₀ for VOC and $\{\text{AP}, \text{AP}_{50}, \text{AP}_{75}, \text{AP}_S, \text{AP}_M, \text{AP}_L\}$ for COCO.

4.2 Benchmark Results

Following (Liu et al. 2022), we compare DISCO with the state-of-the-art methods including FasterRCNN (Ren et al. 2015), RetinaNet (Lin et al. 2017b), FreeAnchor (Zhang et al. 2019), Co-teaching (Han et al. 2018), SD-LocNet (Zhang, Yang, and Feng 2019), KL Loss (He et al. 2019), and OA-MIL (Liu et al. 2022). For reference, we also report the results of Clean-FasterRCNN/RetinaNet, which are trained with clean annotations under the same setup.

The experimental results on VOC and COCO are reported in Table 1. It can be observed that noisy bounding box annotations significantly reduce the performance of vanilla object detectors like FasterRCNN and RetinaNet, especially at high box noise levels. Moreover, Co-teaching and SD-LocNet can only marginally improve detection performance, showing that small-loss sample selection and sample weight assign-

Component			Category																				All
DA-Aug	DA-Ref	DA-Est	Aero	Bicy	Bird	Boat	Bot	Bus	Car	Cat	Cha	Cow	Dtab	Dog	Hors	Mbik	Pers	Plnt	She	Sofa	Trai	Tv	
✓			49.4	69.5	47.4	32.1	35.2	62.3	64.1	60.3	31.9	55.1	41.5	61.8	54.3	56.8	58.7	22.5	48.6	49.7	49.8	51.3	50.1
	✓		56.0	70.6	56.0	38.5	33.0	64.7	74.8	77.4	32.2	58.5	42.4	72.1	65.6	64.8	62.5	23.4	51.2	51.5	65.7	50.5	55.6
		✓	61.2	74.4	59.7	43.1	37.0	69.4	75.2	73.3	34.8	64.1	54.5	74.1	71.7	66.0	66.7	28.7	54.1	55.4	70.5	60.2	59.7
✓	✓		69.9	77.1	68.2	47.2	49.9	70.9	80.6	80.8	43.0	76.4	60.0	82.6	81.0	74.4	73.4	39.2	62.7	64.3	67.9	68.6	66.9
✓	✓	✓	71.5	76.9	71.5	45.6	52.2	76.1	81.2	83.2	43.4	79.8	60.3	81.5	82.9	75.4	73.6	40.6	64.4	68.2	76.8	70.0	68.7

Table 2: Ablation studies of component effectiveness. Note that per-category performance is reported for a detailed comparison.

Hyper.	Value	AP ₅₀	Hyper.	Value	AP ₅₀	Hyper.	Value	AP ₅₀
	0.01	68.6		3	68.3		0.7	68.1
T	0.1	68.7	α	5	68.7	β	0.8	68.7
	0.2	67.8		7	68.2		0.9	67.3

Table 3: Ablation studies of hyperparameter sensitivity.

ment are not decent solutions for handling noisy bounding boxes. Besides, even with better label assignment, FreeAnchor still underperforms in such a challenging task. It is worth noting that KL Loss is a competitive method that also improves the interpretability of detectors. Moreover, OA-MIL adopts a MIL-based training strategy by iteratively constructing object-level bags, attaining better detection performance than the aforementioned methods.

As shown in Table 1, the proposed DISCO, which aims to model spatial distributions of proposals to calibrate the corrupt supervision signals, achieves state-of-the-art performance on these two benchmarks. When encountering low noise levels (i.e., 10% and 20%), DISCO is able to perform competitively. Notably, it can significantly outperform the existing methods at high noise levels (i.e., 30% and 40%), showing that our method is more robust to noisy bounding boxes. Specifically, compared with OA-MIL, DISCO attains $+1.5AP_{50}$ and $+4.9AP_{50}$ improvement on VOC at the 30% and 40% noise levels respectively. Moreover, DISCO can also achieve $+2.6AP$, $+3.1AP_{50}$, and $+4.0AP_{75}$ improvement on COCO at the 40% noise level. It is also worth noting that DISCO is more effective for relatively small objects which are usually treated as hard cases in object detection.

4.3 Ablation Studies

We conduct comprehensive ablation studies including two aspects, i.e., component effectiveness and hyperparameter sensitivity, to further verify the performance improvement of DISCO. Unless otherwise specified, the following experiments are all based on VOC at the 40% noise level.

Component Effectiveness. To investigate the effectiveness of three key techniques in DISCO (i.e., DA-Aug, DA-Ref, and DA-Est), we gradually integrate them into training. Note that the implementation of DA-Est is heavily based on DA-Ref thus it cannot be adopted independently. The experimental results are reported in Table 2, where we also list per-category performance for a detailed comparison. Notably,

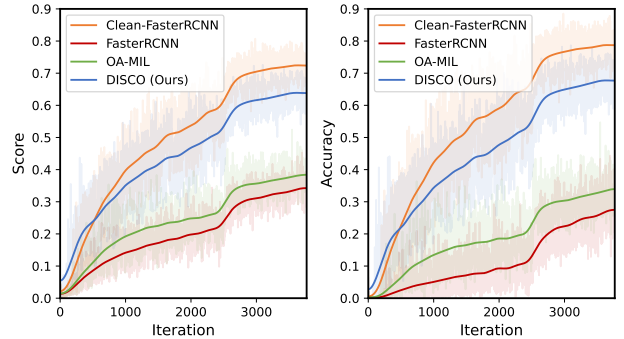


Figure 5: Illustration of classification performance improvement. Left: Average classification scores of the positive proposals for corresponding categories. Right: Classification accuracy of the positive proposals.

using only DA-Aug or DA-Ref can considerably contribute to performance improvement. DA-Ref seems to be more effective since it comes with refined ground-truths for better localization. Moreover, its detection performance can be further boosted when collaborating with DA-Aug or DA-Est. It is also worth noting that DA-Est can achieve $+4.1AP_{50}$ improvement by enhancing the robustness of detectors. Adopting all three techniques, our DISCO can attain superior detection performance in almost all categories, demonstrating the performance improvement of these components.

Hyperparameter Sensitivity. Here we evaluate the sensitivity of T of Equation 6 and α, β of Equation 15, which is relatively crucial for our DISCO. The evaluations of other hyperparameters are provided in the appendix. As shown in Table 3, the temperature coefficient T , which controls the sharpness of the modeled distribution, is relatively robust when set to 0.01 or 0.2. Tuning T to a proper value can contribute to better performance. Moreover, the hyperparameters regulate the fusion of two bounding boxes (i.e., α and β) is also insensitive when varying between a moderate range, showing the effectiveness of our method.

4.4 Further Analysis

In this subsection, additional evidence and discussion are provided to further analyze the advantages of DISCO in classification, localization, and interpretability, respectively. Unless otherwise specified, the following experiments are all based on VOC at the 40% noise level.

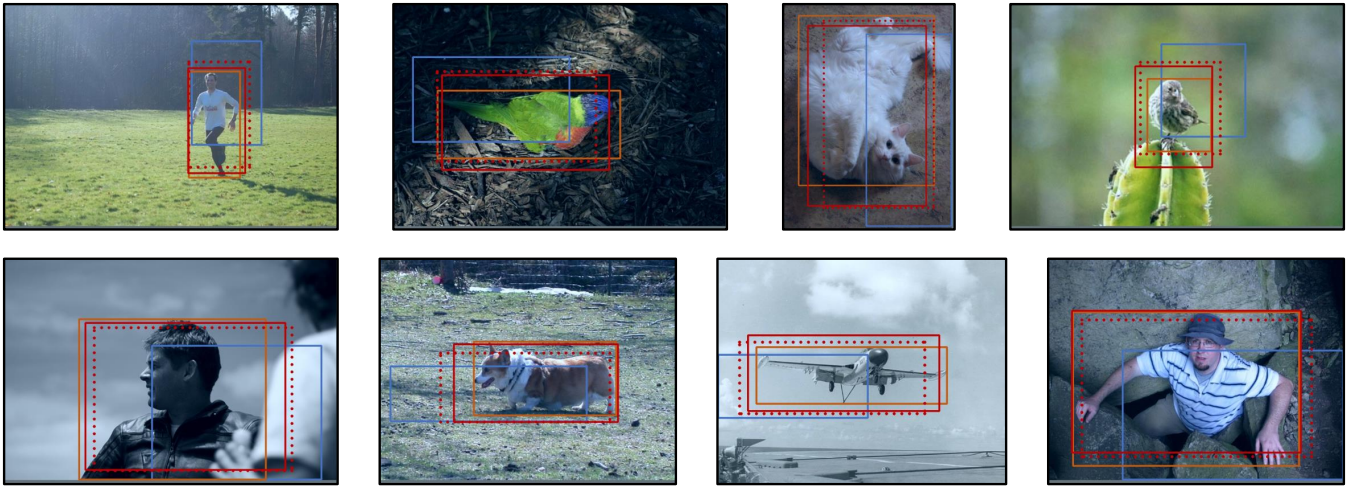


Figure 6: Qualitative results of box refinement in DISCO. Real ground-truths and noisy ground-truths are marked in orange and blue. The refined bounding boxes produced by the first-/second-time DISCO are indicated in dotted/solid red.

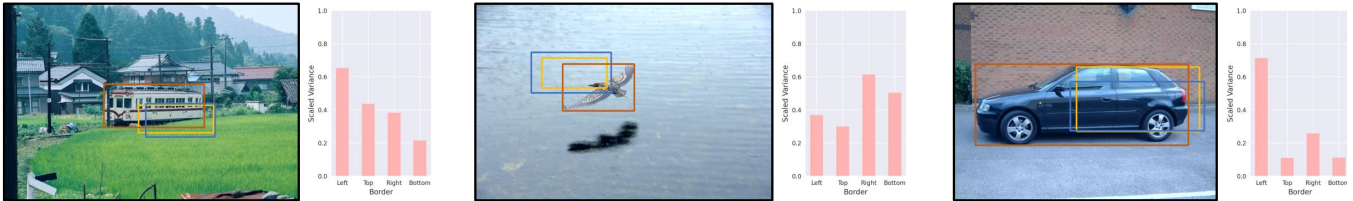


Figure 7: Qualitative results of interpretability in DISCO. We randomly choose an assigned proposal per image to report its predicted variance. Real ground-truths, noisy ground-truths, and proposals are marked in orange, blue, and yellow, respectively. Note that the variance is scaled by the width and height for clarity.

Classification Performance Improvement. In DISCO, DA-Aug is adopted to generate proposals in potential locations of objects for obtaining representative category features, by which classification performance can be further boosted. The evidence is provided in Figure 5. It can be observed that noisy bounding box annotations can badly reduce the classification scores and the accuracy of foreground features. Notably, OA-MIL can also enhance classification performance. More importantly, our DISCO achieves superior improvement for classification, which even approaches the results of training with clean annotations.

Box Refinement for Better Localization. To improve the localization capability of detectors, our DA-Ref utilizes the modeled distributions of proposals for noisy bounding box refinement. Note that DISCO is performed twice in a training iteration and thus there are two successive refined boxes, where the first one is for proposal reassignment and the second one acts as the supervision for regression. As shown in Figure 6, the refined boxes can cover the objects more tightly than noisy ground-truths. Moreover, the second-time refinement contributes to more precise ones, showing the effectiveness of our refinement strategy.

Interpretability with Confidence Estimation. We introduce interpretability into box predictions in DISCO, aiming to enhance the robustness of detectors with a better NMS

(He et al. 2019). This is implemented by estimating the confidence of each border of the predicted bounding boxes with the variance of the modeled distribution as its supervision, because the variance can measure the possibility of potential locations of objects in a border-wise manner. For an intuitive understanding, some qualitative results are represented in Figure 7. For a predicted border that deviates largely from the real one, the detector trained with DISCO could estimate relatively large variance, indicating low confidence for this prediction. Such a crucial property also reflects the practicality of DISCO in realistic scenarios.

5 Conclusions

In this paper, we focus on an under-explored and challenging problem termed object detection with noisy bounding boxes. Motivated by the observation about proposal aggregation, we propose DISCO to model the spatial distribution of proposals for calibrating the corrupt supervision signals. In DISCO, spatial distribution modeling is performed to statistically extract the potential locations of objects, and then three distribution-aware techniques (*i.e.*, DA-Aug, DA-Ref, and DA-Est) are adopted to improve classification, localization, and interpretability, respectively. Experiments show that our DISCO can achieve state-of-the-art performance. We believe that DISCO can serve as a stronger baseline for

this task and expect it can motivate more future works in the field of object detection and learning with noisy labels.

References

- Bilen, H.; and Vedaldi, A. 2016. Weakly supervised deep detection networks. In *Proceedings of the IEEE conference on computer vision and pattern recognition*, 2846–2854.
- Cai, Z.; and Vasconcelos, N. 2018. Cascade r-cnn: Delving into high quality object detection. In *Proceedings of the IEEE conference on computer vision and pattern recognition*, 6154–6162.
- Carion, N.; Massa, F.; Synnaeve, G.; Usunier, N.; Kirillov, A.; and Zagoruyko, S. 2020. End-to-end object detection with transformers. In *European conference on computer vision*, 213–229. Springer.
- Chadwick, S.; and Newman, P. 2019. Training object detectors with noisy data. In *2019 IEEE Intelligent Vehicles Symposium (IV)*, 1319–1325. IEEE.
- Chai, Z.; Luo, L.; Lin, H.; Heng, P.-A.; and Chen, H. 2023. Deep Omni-supervised Learning for Rib Fracture Detection from Chest Radiology Images. *arXiv preprint arXiv:2306.13301*.
- Chen, Z.; Fu, Z.; Jiang, R.; Chen, Y.; and Hua, X.-S. 2020. Slv: Spatial likelihood voting for weakly supervised object detection. In *Proceedings of the IEEE/CVF Conference on Computer Vision and Pattern Recognition*, 12995–13004.
- Choi, J.; Chun, D.; Kim, H.; and Lee, H.-J. 2019. Gaussian yolov3: An accurate and fast object detector using localization uncertainty for autonomous driving. In *Proceedings of the IEEE/CVF International conference on computer vision*, 502–511.
- Diba, A.; Sharma, V.; Pazandeh, A.; Pirsivash, H.; and Van Gool, L. 2017. Weakly supervised cascaded convolutional networks. In *Proceedings of the IEEE conference on computer vision and pattern recognition*, 914–922.
- Everingham, M.; Van Gool, L.; Williams, C. K.; Winn, J.; and Zisserman, A. 2010. The pascal visual object classes (voc) challenge. *International journal of computer vision*, 88: 303–338.
- Girshick, R.; Radosavovic, I.; Gkioxari, G.; Dollár, P.; and He, K. 2018. Detectron.
- Han, B.; Yao, Q.; Yu, X.; Niu, G.; Xu, M.; Hu, W.; Tsang, I.; and Sugiyama, M. 2018. Co-teaching: Robust training of deep neural networks with extremely noisy labels. *Advances in neural information processing systems*, 31.
- He, K.; Gkioxari, G.; Dollár, P.; and Girshick, R. 2017. Mask r-cnn. In *Proceedings of the IEEE international conference on computer vision*, 2961–2969.
- He, K.; Zhang, X.; Ren, S.; and Sun, J. 2016. Deep residual learning for image recognition. In *Proceedings of the IEEE conference on computer vision and pattern recognition*, 770–778.
- He, Y.; Zhu, C.; Wang, J.; Savvides, M.; and Zhang, X. 2019. Bounding box regression with uncertainty for accurate object detection. In *Proceedings of the IEEE/CVF conference on computer vision and pattern recognition*, 2888–2897.
- Hinton, G.; Vinyals, O.; and Dean, J. 2015. Distilling the knowledge in a neural network. *arXiv preprint arXiv:1503.02531*.
- Kantorov, V.; Oquab, M.; Cho, M.; and Laptev, I. 2016. Contextlocnet: Context-aware deep network models for weakly supervised localization. In *Computer Vision—ECCV 2016: 14th European Conference, Amsterdam, The Netherlands, October 11–14, 2016, Proceedings, Part V 14*, 350–365. Springer.
- Li, J.; Xiong, C.; Socher, R.; and Hoi, S. 2020a. Towards noise-resistant object detection with noisy annotations. *arXiv preprint arXiv:2003.01285*.
- Li, X.; Wang, W.; Wu, L.; Chen, S.; Hu, X.; Li, J.; Tang, J.; and Yang, J. 2020b. Generalized focal loss: Learning qualified and distributed bounding boxes for dense object detection. *Advances in Neural Information Processing Systems*, 33: 21002–21012.
- Lin, T.-Y.; Dollár, P.; Girshick, R.; He, K.; Hariharan, B.; and Belongie, S. 2017a. Feature pyramid networks for object detection. In *Proceedings of the IEEE conference on computer vision and pattern recognition*, 2117–2125.
- Lin, T.-Y.; Goyal, P.; Girshick, R.; He, K.; and Dollár, P. 2017b. Focal loss for dense object detection. In *Proceedings of the IEEE international conference on computer vision*, 2980–2988.
- Lin, T.-Y.; Maire, M.; Belongie, S.; Hays, J.; Perona, P.; Ramanan, D.; Dollár, P.; and Zitnick, C. L. 2014. Microsoft coco: Common objects in context. In *Computer Vision—ECCV 2014: 13th European Conference, Zurich, Switzerland, September 6–12, 2014, Proceedings, Part V 13*, 740–755. Springer.
- Liu, C.; Wang, K.; Lu, H.; Cao, Z.; and Zhang, Z. 2022. Robust Object Detection with Inaccurate Bounding Boxes. In *European Conference on Computer Vision*, 53–69. Springer.
- Luo, L.; Chen, H.; Zhou, Y.; Lin, H.; and Heng, P.-A. 2021. Oxnet: Deep omni-supervised thoracic disease detection from chest x-rays. In *Medical Image Computing and Computer Assisted Intervention—MICCAI 2021: 24th International Conference, Strasbourg, France, September 27–October 1, 2021, Proceedings, Part II 24*, 537–548. Springer.
- Mao, J.; Shi, S.; Wang, X.; and Li, H. 2022. 3d object detection for autonomous driving: A review and new outlooks. *arXiv preprint arXiv:2206.09474*.
- Michaelis, C.; Mitzkus, B.; Geirhos, R.; Rusak, E.; Bringmann, O.; Ecker, A. S.; Bethge, M.; and Brendel, W. 2019. Benchmarking robustness in object detection: Autonomous driving when winter is coming. *arXiv preprint arXiv:1907.07484*.
- Pang, J.; Chen, K.; Shi, J.; Feng, H.; Ouyang, W.; and Lin, D. 2019. Libra r-cnn: Towards balanced learning for object detection. In *Proceedings of the IEEE/CVF conference on computer vision and pattern recognition*, 821–830.
- Ren, S.; He, K.; Girshick, R.; and Sun, J. 2015. Faster r-cnn: Towards real-time object detection with region proposal networks. *Advances in neural information processing systems*, 28.

Sun, P.; Zhang, R.; Jiang, Y.; Kong, T.; Xu, C.; Zhan, W.; Tomizuka, M.; Li, L.; Yuan, Z.; Wang, C.; et al. 2021. Sparse r-cnn: End-to-end object detection with learnable proposals. In *Proceedings of the IEEE/CVF conference on computer vision and pattern recognition*, 14454–14463.

Tang, P.; Wang, X.; Bai, X.; and Liu, W. 2017. Multiple instance detection network with online instance classifier refinement. In *Proceedings of the IEEE conference on computer vision and pattern recognition*, 2843–2851.

Uijlings, J. R.; Van De Sande, K. E.; Gevers, T.; and Smeulders, A. W. 2013. Selective search for object recognition. *International journal of computer vision*, 104: 154–171.

Wan, F.; Liu, C.; Ke, W.; Ji, X.; Jiao, J.; and Ye, Q. 2019. C-mil: Continuation multiple instance learning for weakly supervised object detection. In *Proceedings of the IEEE/CVF Conference on Computer Vision and Pattern Recognition*, 2199–2208.

Wan, F.; Wei, P.; Jiao, J.; Han, Z.; and Ye, Q. 2018. Min-entropy latent model for weakly supervised object detection. In *Proceedings of the IEEE conference on computer vision and pattern recognition*, 1297–1306.

Wei, Y.; Shen, Z.; Cheng, B.; Shi, H.; Xiong, J.; Feng, J.; and Huang, T. 2018. Ts2c: Tight box mining with surrounding segmentation context for weakly supervised object detection. In *Proceedings of the European conference on computer vision (ECCV)*, 434–450.

Xu, Y.; Zhu, L.; Yang, Y.; and Wu, F. 2021. Training robust object detectors from noisy category labels and imprecise bounding boxes. *IEEE Transactions on Image Processing*, 30: 5782–5792.

Zhang, H.; Li, F.; Liu, S.; Zhang, L.; Su, H.; Zhu, J.; Ni, L. M.; and Shum, H.-Y. 2022. Dino: Detr with improved denoising anchor boxes for end-to-end object detection. *arXiv preprint arXiv:2203.03605*.

Zhang, X.; Wan, F.; Liu, C.; Ji, R.; and Ye, Q. 2019. Freeanchor: Learning to match anchors for visual object detection. *Advances in neural information processing systems*, 32.

Zhang, X.; Yang, Y.; and Feng, J. 2019. Learning to localize objects with noisy labeled instances. In *Proceedings of the AAAI Conference on Artificial Intelligence*, volume 33, 9219–9226.

Zhu, X.; Su, W.; Lu, L.; Li, B.; Wang, X.; and Dai, J. 2020. Deformable detr: Deformable transformers for end-to-end object detection. *arXiv preprint arXiv:2010.04159*.

Zitnick, C. L.; and Dollár, P. 2014. Edge boxes: Locating object proposals from edges. In *Computer Vision—ECCV 2014: 13th European Conference, Zurich, Switzerland, September 6–12, 2014, Proceedings, Part V 13*, 391–405. Springer.

Zou, Z.; Chen, K.; Shi, Z.; Guo, Y.; and Ye, J. 2023. Object detection in 20 years: A survey. *Proceedings of the IEEE*.

Appendix

A Details of the Experimental Setup

A.1 Noise Simulation

Following (Liu et al. 2022), clean annotations are perturbed to simulate noisy bounding box annotations in our experiments, which is performed once for each dataset. Specifically, let c_x, c_y, w, h represent the central x-axis coordinate, central y-axis coordinate, width, and height of a clean bounding box, respectively. We simulate a noisy bounding box by randomly shifting and scaling a clean one, which can be formulated as

$$\begin{cases} \hat{c}_x = c_x + \Delta_x \cdot w, & \hat{c}_y = c_y + \Delta_y \cdot h, \\ \hat{w} = (1 + \Delta_w) \cdot w, & \hat{h} = (1 + \Delta_h) \cdot h, \end{cases} \quad (20)$$

where $\Delta_x, \Delta_y, \Delta_w,$ and Δ_h obey the uniform distribution $U(-n, n)$ and n is the noise level. For example, when n is set to 40%, $\Delta_x, \Delta_y, \Delta_w,$ and Δ_h would ranges from -0.4 to 0.4 . Note that Equation 20 is conducted on each bounding box of the training set. Such a noise simulation can guarantee access to real ground-truths for analyzing training behaviors and evaluating the performance of box refinement.

A.2 Hyperparameter Selections

There are six hyperparameters in DISCO, including the temperature coefficient T , the augmented proposal number N' , two box fusion hyperparameters α and β , and two loss weights γ and λ . For the sake of simplicity, we empirically fix N' and γ to 10 and 0.3, and then tuning $T \in [0.01, 0.2]$, $\alpha \in [3, 10]$, $\beta \in [0.7, 0.9]$, and $\lambda \in [0.01, 0.2]$. To ensure reproducibility, the selected hyperparameters for all settings are reported in Table 4. Notably, we have just roughly tuned these hyperparameters by selecting some regular values, thus the performance of our method in Table 1 has the potential to be better.

Dataset	Box Noise Level	Hyperparameter					
		T	N'	α	β	γ	λ
VOC	10%	0.05	10	10	0.7	0.3	0.05
	20%	0.05	10	10	0.7	0.3	0.05
	30%	0.1	10	10	0.8	0.3	0.1
	40%	0.1	10	5	0.8	0.3	0.1
COCO	20%	0.01	10	10	0.7	0.3	0.01
	40%	0.1	10	5	0.8	0.3	0.1

Table 4: Hyperparameter selections. We report the hyperparameters for all settings to ensure reproducibility.

B Additional Experiments

B.1 Performance on Different Backbones

As mentioned in Section 4.1, the benchmark experiments are performed with ResNet-50-FPN (He et al. 2016; Lin et al. 2017a) as the backbone. To further demonstrate the

superior performance of our method, we conduct additional benchmark experiments on different backbones. Specifically, DISCO is compared to OA-MIL on COCO at the 40% noise level with the backbone set to ResNet-101-FPN (He et al. 2016; Lin et al. 2017a). In this way, we can evaluate the performance improvement of our DISCO for a large-scale dataset when it is equipped with a larger backbone. The experimental results are reported in Table 5. It can be observed that our DISCO can further improve detection performance and still achieve state-of-the-art results, showing its potential to be coupled with more powerful backbones.

Method	Backbone	AP	AP ₅₀	AP ₇₅	AP _S	AP _M	AP _L
OA-MIL	ResNet-50-FPN	18.6	42.6	12.9	9.2	19.0	26.5
OA-MIL	ResNet-101-FPN	19.3	44.1	13.1	9.3	20.8	27.8
DISCO (Ours)	ResNet-50-FPN	21.2	45.7	16.9	11.4	24.7	27.8
DISCO (Ours)	ResNet-101-FPN	22.7	47.6	18.4	12.9	26.6	29.8

Table 5: Additional benchmark results of DISCO and OA-MIL on COCO with ResNet-101-FPN backbone. Note that we also present the results with ResNet-50-FPN backbone for a clear comparison.

B.2 More Ablation Studies

In this section, we conduct more ablation studies to further verify the effectiveness of the proposed DISCO. These ablation studies contain the execution time of DISCO and sensitivity analysis of other hyperparameters. Unless otherwise specified, the following experiments are all based on VOC at the 40% noise level.

Execution Time of DISCO. In this work, DISCO is performed twice in a training iteration, where the first time is for proposal reassignment and the second time is for obtaining better supervision. We compare such an execution strategy with two other options: 1) One time of DISCO: proposal reassignment is removed and the only one time of DISCO is for obtaining better supervision; 2) Three times of DISCO: the first two times are for proposal reassignment and the third time is for obtaining better supervision. As shown in Table 6, more execution times of DISCO do not contribute to better detection performance. This is because such an improper strategy could result in excessive box refinement and thus influence the learning stability of detectors. Moreover, it also can be observed that our execution strategy can achieve superior performance.

Execution Time of DISCO	AP ₅₀
1	68.1
2	68.7
3	67.9

Table 6: Ablation studies of the execution time of DISCO.

Other Hyperparameter Sensitivity. We perform sensitivity analysis for other hyperparameters, including N' of Equation 9 and γ, λ of Equation 19. Note that we choose some moderate values rather than extreme ones to reasonably evaluate the sensitivity for each hyperparameter. The experimental results are reported in Table 7. It can be observed that the augmented proposal number N' is insensitive when varying from 5 to 20. This is the reason why we empirically fix N' to 10 for all settings. Besides, two loss weights γ, λ also remain insensitive while λ is relatively crucial. This is because it controls the strength of an extra classification loss term, directly affecting classification accuracy.

Hyper.	Value	AP ₅₀	Hyper.	Value	AP ₅₀	Hyper.	Value	AP ₅₀
N'	5	68.5	γ	0.1	68.3	λ	0.05	67.9
	10	68.7		0.3	68.7		0.1	68.7
	20	68.6		0.5	68.4		0.15	67.4

Table 7: Ablation studies of hyperparameter sensitivity.

C More Qualitative Results

C.1 Box Refinement

As an extension to Figure 6, we present more qualitative results of box refinement in DISCO (see Figure 8), which shows that DISCO can attain tighter bounding boxes than noisy ground-truths. As shown in Figure 8, it is worth noting that DISCO can achieve consistent refinement of bounding boxes for different objects varying in size.

C.2 Interpretability

In Figure 9, more qualitative results of interpretability in DISCO are provided to demonstrate such a characteristic of our method. As shown in Figure 9, when trained with DISCO, the detector can output reasonable variance as the confidence for each border of predicted bounding boxes, which shows that the detector is capable of realizing which border may be inaccurately predicted.

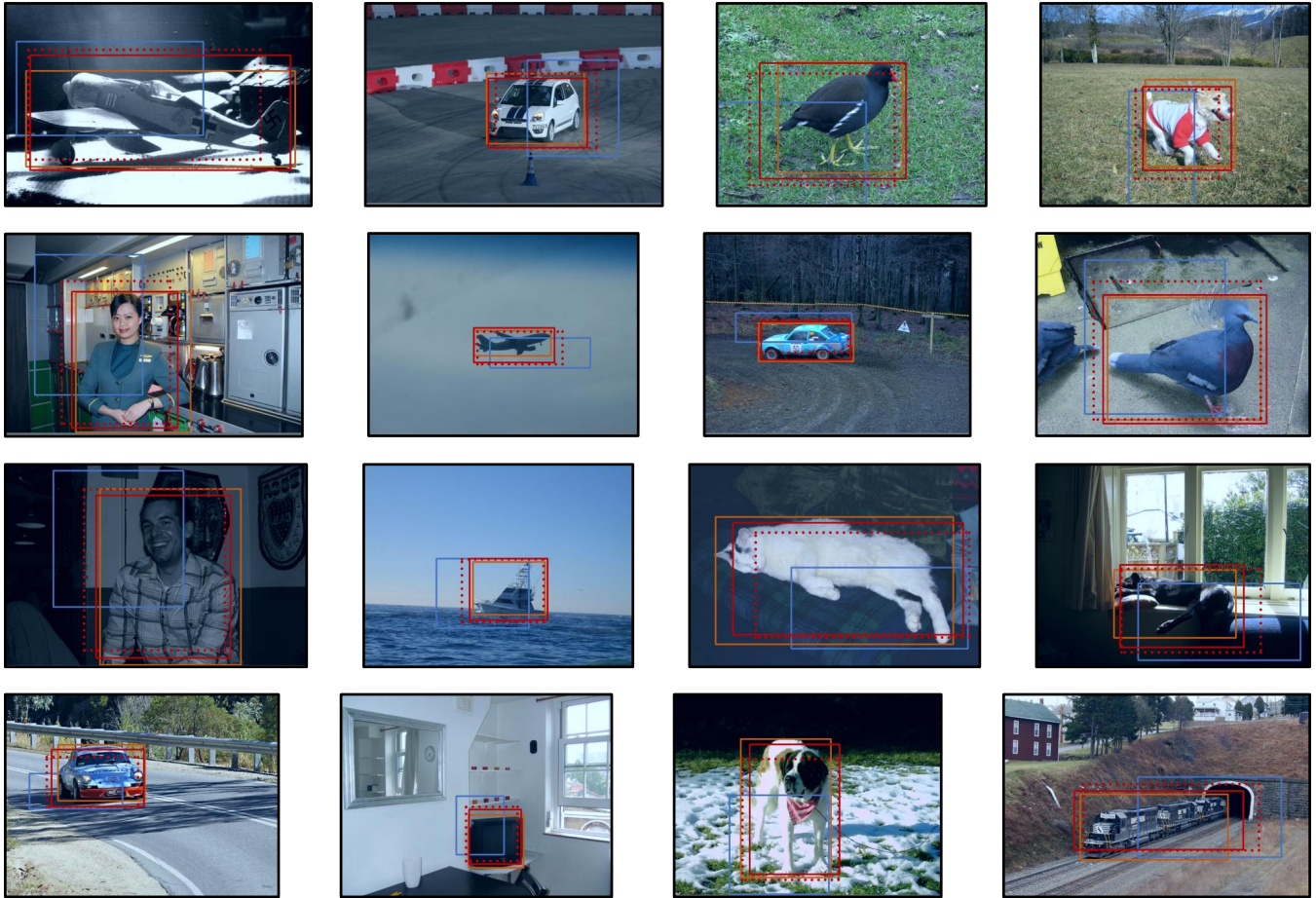


Figure 8: Qualitative results of box refinement in DISCO. Real ground-truths and noisy ground-truths are marked in orange and blue. The refined bounding boxes produced by the first-/second-time DISCO are indicated in dotted/solid red.

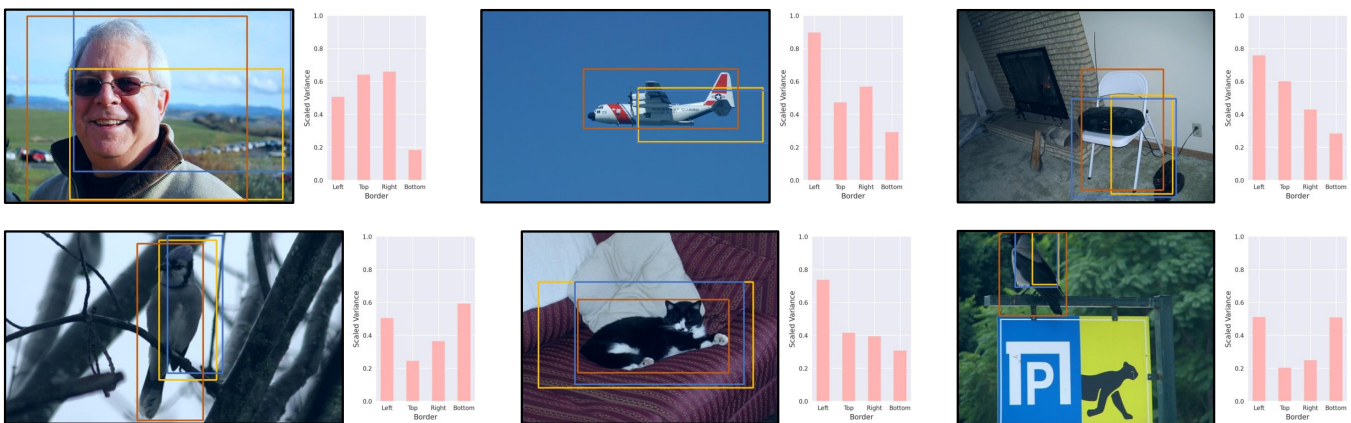


Figure 9: Qualitative results of interpretability in DISCO. We randomly choose an assigned proposal per image to report its predicted variance. Real ground-truths, noisy ground-truths, and proposals are marked in orange, blue, and yellow, respectively. Note that the variance is scaled by the width and height for clarity.